

---

# The evolution of galaxy groups and of galaxies therein

Gary A. Mamon

IAP, 98 bis Bd Arago, F-75014, Paris, France, [gam@iap.fr](mailto:gam@iap.fr)

**Summary.** Properties of groups of galaxies depend sensitively on the algorithm for group selection, and even the most recent catalogs of groups built from redshift-space selection should suffer from projections and inclusion of infalling galaxies. The cosmo-dynamical evolution of groups from initial Hubble expansion to collapse and virialization leads to a fundamental track in virial-theorem estimated  $M/L$  vs crossing time. The increased rates of mergers, both direct and after orbital decay by dynamical friction, in (low velocity dispersion) groups relative to clusters, explain the higher fraction of elliptical galaxies at given local number density in X-ray selected groups, relative to clusters, even when the hierarchical evolution of groups is considered. Galaxies falling into groups and clusters should later travel outwards to typically 2 virial radii, which is close to but somewhat less than the outermost radius where galaxy star formation efficiencies are observed to be enhanced relative to field galaxies of same morphological type. An ongoing analysis of the internal kinematics of X-ray selected groups suggests that the radial profiles of line of sight velocity dispersion are consistent with isotropic NFW distributions for the total mass density, with higher concentrations in massive groups than  $\Lambda$ CDM predictions and lower concentrations in low mass groups. The critical mass, at  $M_{200} \approx 10^{13} M_\odot$  is consistent with possible breaks in the X-ray luminosity-temperature and Fundamental Plane relations. The internal kinematics of groups indicate that the  $M - T$  relation of groups should agree with that extrapolated from clusters with no break at the group scale. The analyses of observed velocity dispersion profiles and of the fundamental track both suggest that low velocity dispersion groups (compact and loose, X-ray emitting or undetected) are quite contaminated by chance projections.

## 1 Introduction

The attractive nature of gravity tends to assemble galaxies together in groups. With typical grouping algorithms, roughly half of all galaxies reside in groups. A smaller fraction of galaxies live in virialized groups of at least 4 bright galaxies, and a considerably smaller fraction live in the more massive virialized clusters.

Given typical scaling relations, defining the virial radius of groups where the mean density is 200 times the critical density of the Universe, groups of galaxies have ranges of mass within the virial radius, virial and turnaround radii (all assuming  $H_0 = 70 \text{ km s}^{-1} \text{ Mpc}^{-1}$ ), velocity dispersion and temperature shown in Table 1. More massive objects can be called clusters. Of course,

**Table 1.** Typical scales of groups

	$\log M_{200}$ ( $M_\odot$ )	$r_{200}$ (Mpc)	$r_{\text{ta}}$ (Mpc)	$\sigma_v$ ( $\text{km s}^{-1}$ )	$kT$ (keV)
Minimum	12.5	0.3	1.1	140	0.2
Maximum	14.0	1.0	3.4	450	2

the limiting mass between groups and clusters is arbitrary and historical. The more massive groups have properties (e.g.  $L_X - T$  [1] and Fundamental Plane [2] relations) expected from the extrapolation of clusters, while the less massive groups do not appear to follow such extrapolations, with the separation between massive cluster-like and low mass groups occurring at  $M_{200} \approx 10^{13} M_\odot$ .

Groups of galaxies thus provide an important laboratory to understand how the density of the environment affects the properties of galaxies. In turn, the modulation with environment of galaxy properties serves as an important constraint for (semi-)analytical models of galaxy formation.

This review focusses on several dynamical and cosmological aspects of the evolution of groups and of their constituent galaxies.

## 2 The evolution of groups

### 2.1 Group expansion, collapse and virialization

Groups are difficult to define from galaxy catalogs, because the selection of nearby galaxies in redshift space causes frequent interlopers and spurious groups [3, 4] (also Eke, at this meeting). This problem of interlopers and spurious groups is probably worsened by the use of the Friends of Friends grouping algorithm, which tends to produce filamentary structures when there are less than a dozen objects (it would be worthwhile to compare the efficiency of the Friends-of-Friends algorithm with other grouping methods, based upon cosmological simulations).

While virialized structures in a  $\Lambda$ CDM Universe with  $\Omega_m = 0.24$  [5] have a mean density  $\Delta = 384$  [6] times the mean density of the Universe, i.e. 94 times the critical density of the Universe, groups have been selected in the past with Friends-of-Friends linking lengths corresponding to an overdensity of only 20 [7] or 80 [8, 9, 10]. In comparison, the mean density at the turnaround

radius in a  $\Lambda$ CDM Universe with  $\Omega_m = 0.24$  is 14 times that of the Universe (Mamon, in preparation). Overdensities of 80 relative to the mean Universe density thus roughly correspond to the geometric mean between the virial and turnaround radii, and thus, *in most catalogs, group galaxies are selected out to the region of rapid infall, and the infalling galaxies bias the group definition, mass estimate and properties*. Given very large galaxy samples, such as SDSS, group selection should be done at  $\Delta = 384$ .

In the extreme, all galaxies of a selected group could be in the infalling region. The departure of such a group from virialization has an important effect on the derived virial mass of the system [11, 12, 13]. Indeed, while it is difficult to compare groups of different scale and cosmo-dynamical state (expansion, collapse, virialization), I had realized that the dimensionless crossing time,  $R/(\sigma_v t)$ , and the dimensionless mass bias, that is mass from the virial theorem divided by true mass,  $R\sigma_v^2/(GM)$ , provide a plane in which the evolution of isolated systems in an expanding Universe follow a *fundamental track* (FT), which is independent of their mass [11, 12, 13]. This track is estimated for the case of a binary system of two extended subgroups of very different masses, with no specific angular momentum. The velocity dispersion of a system can be expressed as  $\sigma_v^2 = (\dot{R})^2 + (\sigma_v)_{\text{proper}}^2$ . The FT, shown in the left panel of Figure 1, was derived assuming that the velocity dispersion of the expanding/collapsing group is dominated by the  $\dot{R}$  term, with the proper velocity dispersion dominating after the full collapse.

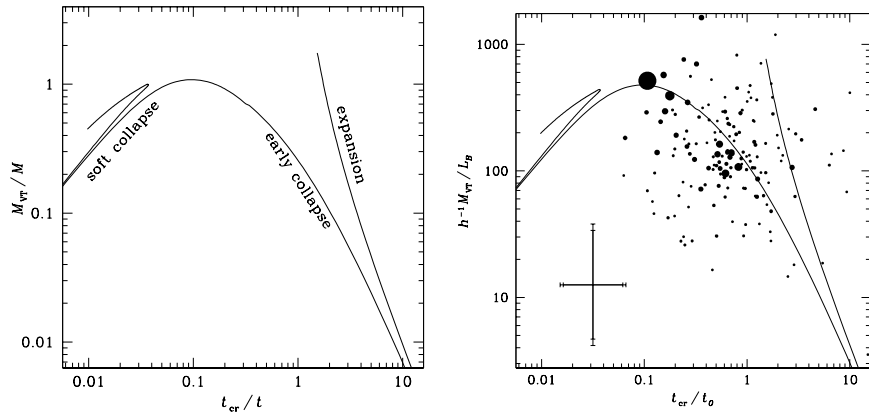


**Fig. 1.** Cosmo-dynamical evolution of galaxy systems (adapted from [11]). The left panel shows the theoretical evolution of an isolated binary with no specific angular momentum and small mass ratio. The right panel shows observed groups [14, 15], with increasingly larger symbols for richer groups. The *thin* and *thick error bars* are for the quartets and typical [14, 15] groups, respectively. The *largest symbol* is the Virgo cluster. The fundamental track was drawn assuming  $M_{\text{true}}/L_B = 440 h$ .

The left panel of Figure 1 shows that the true mass is usually severely underestimated by application of the virial theorem. During the early stages of collapse, this occurs because the velocity dispersion of the system is still low (as  $\dot{R}$  is small). Near full collapse, the galaxies decouple from their dark matter halos: while the virial theorem measures the mass at the radius of the group where lie the galaxies, there is dark matter beyond that radius. The FT diagram (left panel of Fig. 1) also indicates that while the crossing time is to first approximation a good estimator of the cosmo-dynamical evolution of a group, it suffers from degeneracies between the expansion and early collapse phases, and also between the full collapse and rebound phases. These degeneracies can be lifted in part by combining crossing times with the virial to true mass ratio. Note that the precise evolution of a system after full collapse is not well known and probably varies from group to group, depending on the specific angular momentum of the binary.

The right panel of Figure 1 shows how observed groups relate to this FT. Since we do not know the true masses of groups, we assume, as a first order approximation that the optical luminosity of a group is proportional to its true mass. The true mass-to-light ratio is a free parameter and is fitted with the highest multiplicity groups, yielding  $M_{\text{true}}/L_B = 440 h$  (where  $h = H_0 / [100 \text{ km s}^{-1} \text{ Mpc}^{-1}]$ ), while the median  $M_{\text{VT}}/L_B$  is 4 times smaller (because it is dominated by low multiplicity groups near turnaround).

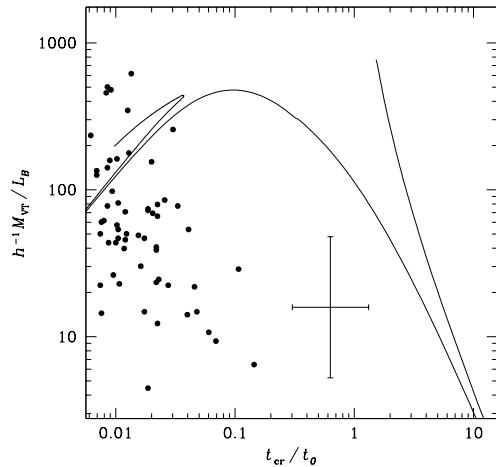
Interestingly, *most groups lie near the fundamental track*. The large scatter for the low multiplicity groups is partly due to larger errors in estimating the plotted quantities given small numbers of galaxies, but the errors are not sufficient in explaining the large number of low-multiplicity groups well below the FT, unless these groups, either have lower  $M/L_B < 440 h$  (because of an intrinsic  $M/L$  increase with group luminosity, or because the galaxies in these particular groups are undergoing bursts of star formation), or are caused by chance alignments of galaxies along the line-of-sight (for which the group radius is underestimated, while the velocity dispersion is not).

Figure 2 displays the positions of Hickson's compact groups [16, 17] relative to the FT. The high velocity dispersion compact groups agree with the predicted FT for  $M_{\text{ture}}/L_B = 440 h$ , while the low velocity dispersion compact groups do not. The strong offset of the low  $\sigma_v$  compact groups relative to the FT can be explained either by bursts of star formation (making  $L_B$  a poor estimator of the true mass) or by chance alignments of galaxies along the line of sight within large collapsing groups [11] (for which the compact group radius is a severe underestimate of the parent group radius).

### 3 The evolution of galaxies in groups

#### 3.1 The many physical processes at work

Dense environments are expected to alter the properties of galaxies. A variety of physical mechanisms are at work in groups and clusters: basically gravita-



**Fig. 2.** Same as right panel of Figure 1, with the same  $M_{\text{true}}/L_B = 440 h$ , but for Hickson compact groups [16, 17]. Velocity dispersion increases from lower right to upper left.

tional and hydrodynamical. We highlight below those processes that alter the morphologies, gas content (and briefly star formation efficiency) of galaxies in groups.

Major galaxy mergers drastically alter the galaxy morphologies, destroying the disks of spirals galaxies and producing a merger remnant that resembles an elliptical galaxy, not only in its surface brightness profile [18], but in the details of its internal kinematics [19]. Minor mergers are expected to build up the bulges of spirals at the expense of their disks [20]. But repeated minor mergers can have the effect of a single major merger [20]. Similarly, repeated minor encounters (merging or not) will “harass” a galaxy enough to substantially transform it [21]. Rapid non-merging encounters also play an important role: the tidal force at closest approach (pericenter) produces a quadrupolar perturbation on the shape of the galaxy, and in extreme cases does the same on its giant molecular clouds. The latter tidal force thus accelerates star formation, while the former can help gas fall into the galaxy core, thus driving an episode of active galactic nucleus (AGN) [22]. In addition to these collisional tides, the galaxy is affected by the mean tidal field of its cluster [23] or dense group [24], where this global tide is more efficient at altering galaxies than the tides from galaxy encounters [24]. The mean tidal field of the group or cluster does not simply limit the galaxy extent and mass, but by pumping energy into the reservoir of outer gas, it suppresses gas infall onto galaxy disks, thus severely reducing long-term star formation [25], a process often called disk strangulation.

Gas can be removed from its parent galaxy through ram pressure ( $P \rho_e v^2$ , where  $\rho_e$  is the gas density of the environment). This idea was first applied to colliding spiral galaxies [26], and later it became clear that the hot intracluster gas provides an important ram pressure [27]. After losing its gas, a spiral galaxy would see its disk fade and resemble a lenticular (S0) galaxy. It is not yet clear that S0s are indeed produced by ram pressure gas stripping, or are simply systems with large bulge to disk ratio. Ram pressure stripping produces the correct local and global trends in clusters [28], but cannot explain the presence of S0s in groups, where the lower velocities are unable to produce sufficiently high ram pressure [29, 30]. On the other hand, if the large bulges of S0s are built up by minor mergers, the fraction of S0s in clusters are found to be lower in semi-analytical models of galaxy formation [31] than observed. However, the inclusion of ram pressure stripping (in very simplistic schemes) does not increase enough the S0 fraction in semi-analytical models [32, 33].

The morphological segregation of galaxies in groups and clusters obviously leads to color segregation, where the redder galaxies lie in the dense central regions, but interestingly, the galaxy colors are redder for given morphological type in clusters than in the field [34], which can be simply explained by the tidal dissipation of the gas reservoirs of spirals [35].

Most of the processes listed here work best in dense environments. On the contrary, for very loose groups such as the Local Group, which are still in the collapse phase, major interactions have not yet altered the more massive galaxies. Only the low mass satellites of massive galaxies are affected by the presence of their more massive companion.

### 3.2 How frequently do group galaxies merge?

The merger rate per unit volume of equal mass galaxies in a group is obtained by integrating over a merger cross-section:

$$k(m) \equiv k(m, m) = \langle vS(v) \rangle = \int_0^\infty vS(v)f(v)dv , \quad (1)$$

where  $S(v) = \pi p_{\text{crit}}^2(v)$  is the relative-velocity dependent merger cross-section and  $f(v)$  is the distribution of relative velocities. For a linear  $p_{\text{crit}}(v)$  [36], one finds [37]

$$k = b \frac{r_h^2 \sigma_g^4}{\sigma_e^3} , \quad (2)$$

where  $r_h$  and  $\sigma_g$  are the half-mass radius and (1D) velocity dispersion of the galaxies,  $\sigma_e$  is the velocity dispersion of the environment, and with now old cross-sections scalings [36, 38] one has  $b \simeq 200$ . With  $\sigma_g^2 \simeq 0.4/3 Gm/r_h$  [39], one then gets [37]

$$k(m) = a \frac{G^2 m^2}{\sigma_e^3} , \quad (3)$$

where  $a \simeq 3.5$ . The merger rate has also been derived directly [40] from fairly realistic  $N$ -body simulations of the mergers of equal mass Hernquist [41] models, and this rate is essentially identical to my analytical prediction [37], as shown in a previous review of mine [42], despite my neglect of gravitational focussing and my use of merger cross-sections based upon very primitive  $N$ -body simulations [36, 38].

In my previous review [42], I've adapted equation (2) to estimate the merger rates for unequal mass galaxies, and integrating over the mass function of field galaxies I derived a merger rate as a function of galaxy mass:

$$\frac{dN_m}{dt} = \text{cst } n_* \frac{G^2 m_*^2}{\sigma_e^3} \mathcal{R} \left( \frac{m}{m_*} \right), \quad (4)$$

where  $m_*$  and  $n_*$  are the break in the galaxy mass function and a fiducial number density, while  $\mathcal{R}(m)$  is a dimensionless function of mass which, for major mergers, increases with mass, reaches a maximum near  $m = m_*$  and decreases sharply for  $m > m_*$ . The normalization is such that  $m_*$  galaxies in typical  $\sigma_v = 300 \text{ km s}^{-1}$  groups should suffer a few major mergers per Hubble time [42]. I also estimated merger rates as a function of position in the group or cluster and found that the direct merger rate outside of the central galaxy is maximum at  $\simeq 0.1 R_{200}$  [42]. An increasing number of observational constraints on the galaxy merger rate and its evolution are now arising (see Conselice in these proceedings and [43]) and need to be compared with the predictions given here.

### 3.3 Do we understand the morphology-density relation in groups and clusters?

The predictions above on the rates of direct mergers versus environment can be compared to the global morphological mix and its local variations (the morphology-density relation, hereafter MDR) observed in groups and clusters. While an early analysis [44] concludes to a universal MDR as a function of local galaxy density, a closer look reveals various problems with groups of galaxies: Hickson's [16] compact groups, assumed as dense in 3D as they appear in 2D, have much higher spiral fractions than expected from the universal MDR [45]. Conversely, these compact groups are spiral-poor relative to other systems of the same velocity dispersion [46], but with a very strong inverse correlation of spiral fraction and velocity dispersion [47], also seen in general SDSS groups [48].

Recently, Helson & Ponman [30] compared the local morphological mix of their sample of X-ray emitting groups to that of clusters [49]. After statistical correction for projections, X-ray emitting groups appear to be spiral-poor relative to clusters of the same local 3D density, by an amount just as expected from the  $\sigma_e^{-3}$  scaling of equations (2) and (3) [30]. In other words, the true groups, as selected by their X-ray emission, have less spirals than clusters

because their lower velocity dispersions lead to slow enough encounters to lead to major mergers that transform spirals into ellipticals.

This simple understanding of the MDR of groups vs clusters has 3 caveats:

1. Major mergers are probably more often the result of orbital decay by dynamical friction than of direct slow collisions. The orbital decay time scales as the dynamical friction (df) time [13], which scales as

$$\left( \frac{dN_m}{dt} \right)_{\text{df}} \propto \tau_{\text{df}}^{-1} \propto \frac{G^2 m \rho}{\sigma_e^3} \ln \left( \frac{M(R)}{m} \right) . \quad (5)$$

Comparing equations (4) and (5), one finds that the rate of direct to frictional mergers scales as  $\ln(M(R)/m)/f$ , where  $f$  is the mass fraction of the group/cluster in galaxies. This small (logarithmic) dependence on the mass of the environment means that *to first order, the ratio of frictional to direct mergers is independent of the environment*, with direct mergers slightly more (less) important in groups (clusters).

2. When two groups or clusters merge, violent relaxation might cause their galaxy populations to mix sufficiently to erase their MDRs. However,  $N$ -body simulations indicate that when two systems merge, there is a strong correlation between initial and final binding energies [50], so that the most bound galaxies in the initial groups or clusters, mostly ellipticals, will end up as the most bound galaxies, thus preserving the MDR.
3. Our analysis pertains to instantaneous merger rates. Since we live in a hierarchical Universe where the rich clusters today were built of smaller groups, we still need to check that the ratio of instantaneous merger rates in groups and clusters is equal to the ratio of the time-averaged merger rates in groups and clusters. But since the merger rates scales as  $\sigma_e^{-3}$ , hence as one over the mass of the environment, the ratio at any time between the merger rates of the main progenitors of present-day groups and clusters will scale as  $M_{\text{group}}(t)/M_{\text{cluster}}(t)$ . Since massive clusters are rare objects, they must form recently, because otherwise they would be even more extreme objects in the past. However, this effect is not too severe: from cosmological  $N$ -body simulations and analytical predictions of the mass assembly history of cosmic systems [51], I infer that the elapsed time for the doubling in mass of (the main progenitors of) present-day groups ( $z = 0.9$ ) is only 1/3 greater than that of present day clusters ( $z = 0.4$ ). Therefore, the average mass ratio of the group to cluster progenitors decreases only slightly with time, so that *to first order the time averaged ratio of merger rates of group and cluster progenitors is close to the ratio of present-day merger rates*.

Therefore, none of the caveats is serious, and it does appear that *the increased rate of galaxy mergers indeed explains the larger local fractions of ellipticals in X-ray selected groups relative to clusters*.

Since compact groups in general are spiral-rich [45], while X-ray selected groups are spiral-poor [30], then *the compact groups that are not in the GEMS*

*sample must be nearly devoid of early-type galaxies*, i.e. the spiral fractions of these groups should be as high or higher than in the average field. The non-X-ray emitting compact groups are typically low velocity dispersion groups, which as we saw, do not fit the FT, so it is tempting to conclude that *low velocity dispersion compact groups are mostly caused by chance projections*.

### 3.4 How far out should galaxies feel the group environment?

The decreased star formation rate for group/cluster galaxies of given morphological type is visible out to  $2r_{200}$  [34], i.e.  $\approx 2.6 r_{100}$ . Regardless of whether the mass assembly of groups and clusters is viewed in a monolithic spherical infall context or in a hierarchical merging one, the effects of the group/cluster on the galaxies should thus be seen out to the maximum *rebound* or *backsplash* radius. If this radius is assimilated to the radius of mixing in the spherical infall model, one finds  $r_{\text{reb}} \approx r_{\text{vir}}$  [52]. If one assumes values for the ratio of the (lagrangian) rebound to turnaround radius (e.g. 1/2), and for the corresponding ratio of rebound to turnaround times (e.g. 3/2), one can solve in the context of a flat Universe with a cosmological constant for the rebound radius, and we find  $r_{\text{reb}}/r_{100} \approx 1$  with a maximum of 2.5 for the most favorable case (rebound radius equals turnaround radius and rebound time equals twice the turnaround time) [52]. Deriving reasonable ratios from particle trajectories of an  $\Lambda$ CDM simulation [53], we obtain  $r_{\text{reb}}/r_{100}$  ranging from 0.55 to 1.25 [52]. Finally we considered the final output ( $z = 0$ ) of a GALICS galaxy formation simulation [54] built on top of a dark matter only  $\Lambda$ CDM cosmological simulation, where galaxies penetrating groups and clusters are selected by empty halos (a feature of GALICS is that when halos merge, galaxies remain with the more massive halo). We then found that galaxies (empty halos) travel out to  $1.7 r_{100}$  [52]. These numbers were confirmed through an analysis of the particle trajectories in  $\Lambda$ CDM halos, which shows that particles that penetrate deep into their halo travel out to  $2r_{100}$  [55]  $\simeq 2.6 r_{200}$ . These maximum rebound radii are thus somewhat larger (by 30%) than the observed maximum radius for decreased star formation, but consistent this value.

## 4 The internal kinematics of groups

Clusters of galaxies are beginning to reveal their mass profiles, through analyses of their internal kinematics, X-ray gas or lensing properties. Kinematical analyses are often based upon the Jeans equation of hydrostatic equilibrium, relating the divergence of the anisotropic dynamical pressure tensor with the tracer density times the gradient of the gravitational potential. In spherical symmetry this becomes

$$\frac{d(\nu\sigma_r^2)}{dr} + 2\beta\frac{\nu\sigma_r^2}{r} = -\nu\frac{GM(r)}{r^2}, \quad (6)$$

where  $\nu(r)$ ,  $M(r)$  and  $\beta(r)$  are the radial profiles of tracer number density, total mass, and velocity anisotropy  $\beta = 1 - \sigma_\theta^2/\sigma_r^2$  (where  $\beta = 1, 0$ , and  $\rightarrow -\infty$  corresponds to radial, isotropic and circular orbits, respectively). Since the data are seen in projection, one has to couple the Jeans equation with the anisotropic projection equation [56]

$$\Sigma(R) \sigma_{\text{los}}^2(R) = 2G \int_R^\infty \left(1 - \beta \frac{R^2}{r^2}\right) \nu \sigma_r^2 \frac{r \, dr}{\sqrt{r^2 - R^2}}, \quad (7)$$

where  $\Sigma(R)$  is the surface number density as a function of projected radius  $R$ , and  $\sigma_{\text{los}}(R)$  is the line of sight velocity dispersion profile (hereafter VDP).

For example, assuming isotropic to moderately radial orbits, the mass profile of clusters is consistent with being proportional to the galaxy number density profile [57], which itself was consistent with the cuspy NFW [58] profile. Recently, the mass-anisotropy degeneracy, inherent in the Jeans equation, was recently (partially) lifted: the early type galaxies in clusters follow isotropic orbits [59, 60], galaxy velocities are isotropic in groups and somewhat radial in clusters [61].

Andrea Biviano and I are currently performing a similar analysis for groups of galaxies, as we wish to check if various types of groups (hot vs. cold, etc.) display similar mass profiles and concentrations. For this, we use the GEMS group sample [1], which considers all groups for which there have been X-ray pointings. In this review, we focus on the groups with diffuse X-ray emission distinct from diffuse emission around the central bright elliptical.

We selected group member galaxies with NED (which at the time included the SDSS-DR4 and the 6dFGS-DR2), searching out to twice (to be conservative) a 1st-order estimate of their virial radius,  $r_{200}$  (where the mean density is 200 times the critical density of the Universe) using  $r_{200}/\text{Mpc} = \sigma_v/450 \text{ km s}^{-1}$ , as appropriate for pure NFW models with  $c = 8$  and  $H_0 = 70 \text{ km s}^{-1} \text{ Mpc}^{-1}$  (when  $\sigma_v < 300 \text{ km s}^{-1}$ , we used  $\sigma_v = 300 \text{ km s}^{-1}$  to be conservative) and out to  $\pm 5 \sigma_v$ . We then computed the velocity dispersion and iterated with a  $\pm 3 \sigma_v$  depth.

#### 4.1 Which is the best estimator of virial radius?

Since groups have few galaxies, we need to stack them, normalizing the radii to their virial radius,  $r_{200}$  (as first done by [62]), and similarly stack their velocities to  $V_{200}$ , the circular velocity at  $r_{200}$ . We have considered several estimators of the virial radius: 1) the velocity dispersion, assuming an isotropic pure NFW model with a  $\Lambda$ CDM concentration parameter,  $\sigma$ -NFW; 2) the  $K$ -band total galaxy luminosity, taken from the 2MASS survey, corrected for incompleteness, using an  $M - L_K$  relation [63]; 3) the X-ray emission-weighted temperature, using  $M - T$  relations from several authors [64, 65, 66]. For each of our  $r_{200}$  estimators, we performed the interloper removal, first group per group, then on the stacked pseudo-group. We also removed a few groups

contaminated by nearby groups or clusters and these with  $< 5$  members. In the stacking, we have weighted the galaxies inversely proportional to the number of galaxies in the group out to the virial radius. This weighting gives equal weight to each group in the stacked pseudo-group.

Figure 3 compares the measured VDPs with the expectation from the isotropic Jeans equation [67]:

$$\Sigma(R) \sigma_{\text{los}}^2(R) = 2 G R \int_R^\infty \sqrt{1 - \frac{R^2}{r^2}} \nu(r) M(r) \frac{dr}{r} . \quad (8)$$

We are also investigating other simple anisotropy profiles for which the term in the square root is replaced by other kernels given by [68], and alternatively, we are directly estimating the mass profile for given anisotropy profiles using the recently discovered mass inversion technique [69].

The Sanderson et al. [65]  $M - T$  relation, which predicts lower mass groups than when extrapolated from cluster  $M - T$  relations, appears inconsistent with isotropic NFW models, as the virial radius and velocity dispersion appear to be overestimated by a factor 1.3, i.e. the mass is a factor of 2 higher than predicted from their  $M - T$  relation. A maximum likelihood analysis at  $\beta = \text{cst}$  suggests that the Sanderson et al.  $M - T$  relation can only be reconciled with a highly concentrated ( $c \approx 100$ ) and tangentially anisotropic ( $\beta \approx -2$ ) system. On the other hand, the virial radii built upon  $M - T$  relations derived for hot clusters [66] or cosmological simulations [64] produce velocity dispersion profiles that are consistent with isotropic NFW models. Therefore, *the  $M - T$  relation of groups of galaxies appears to lie in the extrapolation of that of clusters*, with no break at  $\approx 10^{13} M_\odot$ .

## 4.2 Constraints on group mass profiles

We have subdivided the  $G$  groups into subclasses according to their velocity dispersion,  $\sigma_v$ , temperature,  $T$ , ratio of galaxy orbital to gas thermal energies  $\beta_{\text{spec}} = \sigma_v^2 / (kT / \mu m_p)$ , X-ray luminosity,  $L_X$  and  $K$ -band luminosity,  $L_K$ . Figure 4 shows plots analogous to those in Figure 3, but when the sample is subdivided into dynamically hot ( $\sigma_v > 300 \text{ km s}^{-1}$ ) and cold ( $\sigma_v \leq 300 \text{ km s}^{-1}$ ) groups. Regardless of the method used to estimate  $r_{200}$ , *the dynamically hot (cold) groups are always more (less) concentrated in total mass than the  $\Lambda$ CDM prediction for isotropic orbits*. While clusters of galaxies display mass concentrations that are consistent with the  $\Lambda$ CDM predictions ([66] using X-rays and [70, 59, 60, 71] using internal kinematics), the richer (high velocity dispersion) groups appear to be more concentrated than  $\Lambda$ CDM predictions, while the poorer (low velocity dispersion) groups appear to be less concentrated than  $\Lambda$ CDM predictions. The high concentrations of the hot groups are caused in part by fitting the total mass density profile, while the more concentrated baryonic (Sérsic) component gives the illusion of high total mass concentrations [72]. Note that the galaxy distribution is

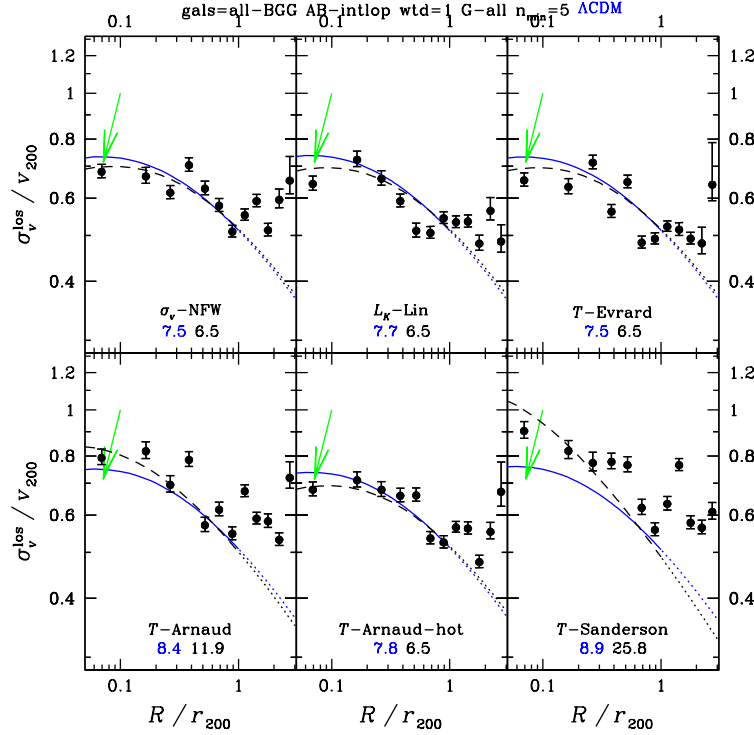


**Fig. 3.** Line-of-sight velocity dispersion profiles for GEMS groups with diffuse emission, drawn for 6 samples stacked using different methods for estimating the virial radius. The curves are the predictions (eq. [8]) for isotropic systems with NFW profiles: total mass and number number densities following  $\Lambda$ CDM predictions (*solid (blue)*), as well as different NFW fits to total mass and number density profiles (*dashed (black)*). The *dotted curves* show the extrapolations beyond the last fitted radius ( $R = r_{200}$ ). The *arrows* indicate the effect of underestimating the virial radius by a factor 1.4. The *labels* at the bottom indicate the method to estimate  $r_{200}$ , where *T-Arnaud-hot* refers to the fit to the hotter clusters of the Arnaud et al. sample. The *numbers under the labels* indicate the concentration parameters for the  $\Lambda$ CDM model and the best NFW fit to the total mass density.

even more concentrated, leading to rising mass over number ratio, consistent with what was derived on an optically selected sample [62]. Alternatively, hot (cold) groups could have  $\Lambda$ CDM mass profiles, with radial (tangential) galaxy orbits. Finally, the strong scatter in the VDPs of the dynamically cold groups suggests that *dynamically cold groups are contaminated by unreal groups*.

There are also strong differences between groups with high and low  $\beta_{\text{spec}}$ , and X-ray luminosity, but smaller differences when subdividing groups into classes of high and low X-ray temperature or *K*-band luminosity.

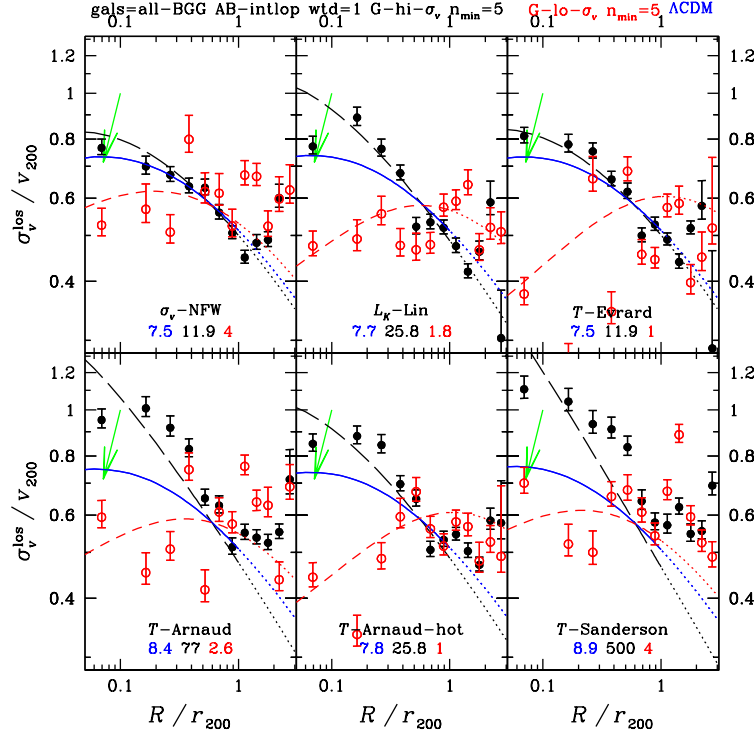


**Fig. 4.** Same as Figure 3, with *long-dashed* (black) and *short-dashed* (red) curves displaying the fits for the dynamical hot ( $\sigma_v > 300 \text{ km s}^{-1}$ ) and cold ( $\sigma_v \leq 300 \text{ km s}^{-1}$ ) groups. The *three numbers under the labels* give the NFW concentration parameters for the  $\Lambda$ CDM model as well as the best fit to the total mass density profiles of the dynamical hot and cold groups, respectively.

#### 4.3 The fundamental track of groups selected to the virial radius

Figure 5 shows the FT of GEMS groups, which were selected out to the virial radius, here defined with the  $L_K$  luminosity. The rich groups cluster near the position expected for virialized systems (the kink of the FT at  $t_{\text{cr}} = 0.035 t_0$ ). Interestingly, the groups that lie off the FT (at lower  $M_{\text{FT}}/L_K$ ) have typically low  $\beta_{\text{spec}}$ , but also longer crossing times. This suggests that these low velocity dispersion groups are not simply low mass-to-light ratio systems, but that there is an intrinsic property that takes them off the FT. The simplest explanation is that *low velocity dispersion groups (compact or not) are chance alignments of galaxies along the line of sight, i.e. prolate groups in real space*.

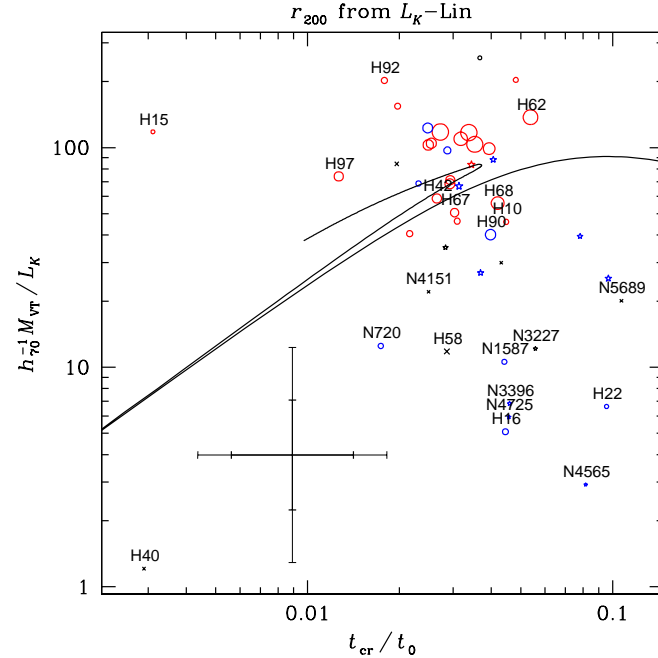


**Fig. 5.** Same as right panel of Figure 1, for GEMS groups selected out to the virial radius (defined with the  $K$ -band luminosity [63]). The *open symbols*, *stars* and *crosses* indicate the GEMS G (extended X-ray emission distinct from central galaxy emission), H (extended X-ray emission indistinguishable from that of central galaxy) and U (undetected extended X-ray emission) groups, respectively. The *red*, *blue* and *black symbols* are for high ( $> 0.5$ ), low ( $\leq 0.5$ ) and undefined (unavailable temperature)  $\beta_{\text{spec}}$ , respectively. The FT was placed assuming the universal value  $M/L_K = 84 h_{70}$  as derived from the  $K$ -band luminosity density of the 6dFGS galaxies [73]. The *symbol sizes* are proportional to the square root of the number of galaxies within  $r_{200}$ . Outliers to the FT and Hickson compact groups are highlighted.

## 5 Concluding thoughts

Our understanding of the evolution of groups and of galaxies therein is making rapid progress thanks to the advent of 1) large galaxy surveys such as the 2dFGRS and SDSS, 2) multi-wavelength observations of groups, and 3) high resolution cosmological  $N$  body simulations. Many of the results presented here need to be confirmed with these large data sets and simulation outputs.

I am grateful to my collaborator, Andrea Biviano, for allowing me to mention our work in progress. I also thank Ivo Saviane, Valentin Ivanov and Jordanka Borissova for organizing a very exciting and high-level meeting and for being extremely patient with the manuscript.

## References

1. J.P.F. Osmond, T.J. Ponman: MNRAS **350**, 1511 (2004)
2. R. Schaeffer, S. Maurogordato, A. Cappi, F. Bernardeau: MNRAS **263**, L21 (1993)
3. B. Moore, C.S. Frenk, S.D.M. White: MNRAS **261**, 827 (1993)
4. A. Diaferio, G. Kauffmann, J.M. Colberg, S.D.M. White: MNRAS **307**, 537 (1999 )
5. D.N. Spergel, R. Bean, O. Doré, et al.: ApJ submitted, arXiv:astro-ph/0603449 (2006)
6. T. Kitayama, Y. Suto: ApJ **469**, 480 (1996)
7. M.J. Geller, J.P. Huchra: ApJS **52**, 61 (1983)
8. M. Ramella, M.J. Geller, J.P. Huchra: ApJ **344**, 57 (1989)
9. M. Merchán, A. Zandivarez: MNRAS **335**, 216 (2002)
10. M.E. Merchán, A. Zandivarez: ApJ **630**, 759 (2005)
11. G.A. Mamon: Dynamical theory of groups and clusters of galaxies. In: *Gravitational Dynamics and the N-Body Problem*, ed by F. Combes, E. Athanassoula (Obs. de Paris, Paris 1993) pp 188–203, arXiv:astro-ph/9308032
12. G.A. Mamon: The galaxy group/cosmology connections. In: Moriond Astrophysics Mtg number 14, *Clusters of Galaxies*, ed by F. Durret, A. Mazure, S.D.M. White, J. Trân Thanh Vân (Frontières, Gif-sur-Yvette 1994) pp 291–296, arXiv:astro-ph/9406043
13. G.A. Mamon: The dynamics of groups and clusters of galaxies and links to cosmology. In: 3rd Paris cosmology colloq, ed by H. de Vega, N. Sánchez (World Scientific, Singapore 1995) pp 95–119, arXiv:astro-ph/9511101
14. P. Fouqué, E. Gourgoulhon, P. Chamaraux, G. Paturel: A&AS **93**, 211 (1992)
15. E. Gourgoulhon, P. Chamaraux, P. Fouqué: A&A **255**, 69 (1992)
16. P. Hickson: ApJ **255**, 382 (1982)
17. P. Hickson, C. Mendes de Oliveira, J.P. Huchra, G.G. Palumbo: ApJ **399**, 353 (1992)
18. J.E. Barnes: ApJ **331**, 699 (1988)
19. A. Dekel, F. Stoehr, G.A. Mamon, T.J. Cox, G.S. Novak, J.R. Primack: Nature **437**, 707 (2005)
20. F. Bournaud, C.J. Jog, F. Combes: A&A **437**, 69 (2005)
21. B. Moore, N. Katz, G. Lake, A. Dressler, A. Oemler, Jr.: Nature **379**, 613 (1996)
22. G.G. Byrd, M.J. Valtonen, L. Valtaoja, B. Sundelius: A&A **166**, 75 (1986)
23. D. Merritt: ApJ **276**, 26 (1984)
24. G.A. Mamon: ApJ **321**, 622 (1987)
25. R.B. Larson, B.M. Tinsley, C.N. Caldwell: ApJ **237**, 692 (1980)
26. L.J. Spitzer, W. Baade: ApJ **113**, 413 (1951)
27. J.E. Gunn, J.R. Gott: ApJ **176**, 1 (1972)
28. J.M. Solanes, E. Salvador-Solé: ApJ **395**, 91 (1992)
29. A. Dressler: ApJ **301**, 35 (1986)
30. S.F. Helsdon, T.J. Ponman: MNRAS **339**, L29 (2003)
31. V. Springel, S.D.M. White, G. Tormen, G. Kauffmann: MNRAS **328**, 726 (2001)
32. T. Okamoto, M. Nagashima: ApJ **587**, 500 (2003)
33. B. Lanzoni, B. Guiderdoni, G.A. Mamon, J. Devriendt, S. Hatton: MNRAS **361**, 369 (2005)
34. M.L. Balogh, D. Schade, S.L. Morris, H.K.C. Yee, R.G. Carlberg, E. Ellingson: ApJL **504**, L75 (1998)

35. M.L. Balogh, J.F. Navarro, S.L. Morris: *ApJ* **540**, 113 (2000)
36. N. Roos, C.A. Norman: *A&A* **76**, 75 (1979)
37. G.A. Mamon: *ApJL* **401**, L3 (1992)
38. S.J. Aarseth, S.M. Fall: *ApJ* **236**, 43 (1980)
39. L. Spitzer: *ApJL* **158**, L139 (1969)
40. J. Makino, P. Hut: *ApJ* **481**, 83 (1997)
41. L. Hernquist: *ApJ* **356**, 359 (1990)
42. G.A. Mamon: Theory of galaxy dynamics in clusters and groups. In: 15th IAP Astrophys. Mtg., *Dynamics of Galaxies: from the Early Universe to the Present*, vol 197, ed by F. Combes, G.A. Mamon, V. Charmandaris (ASP, San Francisco 2000) pp 377–387, arXiv:astro-ph/9911333
43. C.J. Conselice: *ApJ* **638**, 686 (2006)
44. M. Postman, M.J. Geller: *ApJ* **281**, 95 (1984)
45. G.A. Mamon: *ApJ* **307**, 426 (1986)
46. P. Hickson, H.J. Rood: *ApJL* **331**, L69 (1988)
47. P. Hickson, E. Kindl, J.P. Huchra: *ApJ* **331**, 64 (1988)
48. S.M. Weinmann, F.C. van den Bosch, X. Yang, H.J. Mo: *MNRAS* **366**, 2 (2006)
49. A. Dressler, A.J. Oemler, W.J. Couch, et al.: *ApJ* **490**, 577 (1997)
50. J.E. Barnes: *ApJ* **393**, 484 (1992)
51. F.C. van den Bosch: *MNRAS* **331**, 98 (2002)
52. G.A. Mamon, T. Sanchis, E. Salvador-Solé, J.M. Solanes: *A&A* **414**, 445 (2004)
53. T. Fukushige, J. Makino: *ApJ* **557**, 533 (2001)
54. S. Hatton, J. Devriendt, S. Ninin, F.R. Bouchet, B. Guiderdoni, D. Vibert: *MNRAS* **343**, 75 (2003)
55. S.P.D. Gill, A. Knebe, B.K. Gibson: *MNRAS* **356**, 1327 (2005)
56. J. Binney, G.A. Mamon: *MNRAS* **200**, 361 (1982)
57. R.G. Carlberg, H.K.C. Yee, E. Ellingson: *ApJ* **478**, 462 (1997)
58. J.F. Navarro, C.S. Frenk, S.D.M. White: *ApJ* **462**, 563 (1996)
59. E.L. Lokas, G.A. Mamon: *MNRAS* **343**, 401 (2003)
60. P. Katgert, A. Biviano, A. Mazure: *ApJ* **600**, 657 (2004)
61. A. Mahdavi, M.J. Geller: *ApJ* **607**, 202 (2004)
62. R.G. Carlberg, H.K.C. Yee, S.L. Morris, et al.: *ApJ* **552**, 427 (2001)
63. Y.T. Lin, J.J. Mohr, S.A. Stanford: *ApJ* **591**, 749 (2003)
64. A.E. Evrard, C.A. Metzler, J.F. Navarro: *ApJ* **469**, 494 (1996)
65. A.J.R. Sanderson, T.J. Ponman, A. Finoguenov, E.J. Lloyd-Davies, M. Markevitch: *MNRAS* **340**, 989 (2003)
66. M. Arnaud, E. Pointecouteau, G.W. Pratt: *A&A* **441**, 893 (2005)
67. P. Prugniel, F. Simien: *A&A* **321**, 111 (1997)
68. G.A. Mamon, E.L. Lokas: *MNRAS* **363**, 705 (2005)
69. G.A. Mamon, G. Boué: *MNRAS* to be submitted (2006)
70. A. Biviano, M. Girardi: *ApJ* **585**, 205 (2003)
71. E.L. Lokas, R. Wojtak, S. Gottlöber, G.A. Mamon, F. Prada: *MNRAS* **367**, 1463 (2006)
72. G.A. Mamon, E.L. Lokas: *MNRAS* **362**, 95 (2005)
73. D.H. Jones, B.A. Peterson, M. Colless, W. Saunders: *MNRAS* **369**, 25 (2006)